SIMORGH-SHM: A Novel Software for Fully Automated and Precise Fracture Monitoring Based on Acoustic Emission Localization and Moment Tensor Inversion

SEYYEDMAALEK MOMENI, THOMAS SCHUMACHER, NUMA BERTOLA, NESRINE YOUSFI, LINDSAY LINZER, ERNST NIEDERLEITHINGER, EUGEN BRÜHWILER and BRICE LECAMPION

ABSTRACT

Passive ultrasonic stress wave, or acoustic Emission (AE), monitoring is a highly effective technique for continuously assessing the structural health of materials, aiding in the prevention of potential failures. AE refers to elastic waves generated during fracture processes, which are detected and recorded by ultrasonic transducers. Quantitative geophysics-based methods enable processing of recorded waveforms to monitor and characterize the spatio-temporal growth of fractures in brittle materials such as concrete and composites. Due to the complexity of the recorded elastic signals and the non-homogeneous nature of the medium, data processing is often performed manually. The high processing costs associated with large datasets, often exceeding terabytes, have limited the practical application of this approach in real-world scenarios. Therefore, an automated methodology is required to reduce costs while maintaining high precision, enabling its integration into Structural Health Monitoring (SHM) and Non-Destructive Evaluation (NDE) frameworks.

This paper presents the application of a novel automated and high-precision AE monitoring algorithm and software, SIMORGH-SHM, designed for applications ranging from materials testing to seismicity. The software is compatible with various standard data formats and is capable of processing both trigger-based and continuous data streams. After introducing the software package, initial results from AE monitoring of a 4.2-meter-long Ultra-High-Performance Fiber-Reinforced Cementitious Composite (UHPFRC) T-beam are discussed. The beam was equipped with 24 novel embedded ultrasonic transducers and tested in EPFL's Structures Laboratory under cyclic loading to failure. Source localizations were performed and damage mechanisms were estimated using Moment Tensor Inversion (MTI) techniques.

Seyyedmaalek Momeni,* Nesrine Yousfi, and Brice Lecampion, Geo-Energy Laboratory, Gaznat chair on Geo-Energy, EPFL. Station 18, CH-1015, Lausanne, Switzerland
Thomas Schumacher, Civil & Environmental Engineering, Portland State University, Portland, OR 97201, Portland, USA
Numa Bertola, University of Luxembourg, Department of Engineering, Avenue de la Fonte 6, Esch-Sur-Alzette 4364, Luxembourg
Lindsay Linzer, SRK Consulting Ltd, 265 Oxford Road, Illovo, Johannesburg, 2196, South Africa
Ernst Niederleithinger, Bundesanstalt für Materialforschung und -prüfung, Berlin, Germany
Eugen Brühwiler, Ecole Polytechnique Fédérale de Lausanne (EPFL), ENAC IIC, Structures Group, 1015 Lausanne, Switzerland
*Corresponding author (email: seyyedmaalek.momeni@epfl.ch)

INTRODUCTION

The integration of Ultra-High-Performance Fibre-Reinforced Cementitious Composites (UHPFRC) in structural health monitoring represents a significant advancement in modern construction materials. UHPFRC exhibits outstanding mechanical performance, with tensile strengths up to 16 MPa and compressive strengths reaching 200 MPa [1–3], alongside a high modulus of elasticity (~45 GPa) and strain-hardening behavior in tension [4]. These properties make it particularly suited for both new structures and rehabilitation of aging infrastructure [5,6]. Additionally, UHPFRC shows rapid development of mechanical properties due to its low water/binder ratio and unique hydration behavior [7,8], although its hydration degree remains relatively low at 28 days [9,10]. Given these complex behaviors and sensitivity to early-age conditions, precise and continuous monitoring is essential.

Ultrasonic stress wave-based techniques, both passive and active, offer a robust, non-destructive approach to monitor UHPFRC behavior under various load conditions. Passive ultrasonic stress wave (or AE) monitoring captures spontaneous microcracking events [11–16], while active ultrasonic stress wave monitoring enables targeted evaluation of evolving internal properties such as modulus of elasticity and hydration development [17-21, 27]. When combined, these methods provide a comprehensive understanding of damage initiation and propagation across scales. For instance, studies using AE in dogbone and beam specimens have demonstrated that fiber content and curing methods significantly affect cracking patterns and toughness [11,17,14,16]. The integration of passive and active AE techniques at full scale enables the first-time monitoring of UHPFRC early-age properties in situ, crucial for optimizing performance and ensuring long-term structural safety.

In this paper, we investigate the possibility of real-time, high-precision monitoring of the fracture evolution in UHPFRC. AE monitoring is particularly well suited for this purpose, as it captures the elastic waves generated by microcracking and damage processes. These signals, which are recorded by transducers, can be analyzed to map the spatio-temporal growth of fractures. However, due to the complex nature of elastic wave propagation, signal interpretation is often performed manually, and thus time-consuming, and costly. Moreover, the sheer volume of data, scaling linearly with the number of transducers and easily reaching terabytes, forces many studies to downsample signals or use fewer transducers, leading to limited diagnostics and potential safety risks. These limitations highlight the urgent need for automated and scalable solutions that maintain precision while reducing manual workload and costs.

To address these challenges, a novel algorithm and software, SIMORGH-SHM [22-25], has been developed. This high-precision AE monitoring tool enables automatic real-time analysis of both trigger-based and continuous data streams and compatible with standard formats in SHM and NDE contexts. In this study, SIMORGH-SHM is applied to AE data recorded from a 4.2-meter-long UHPFRC T-beam equipped with 24 embedded ultrasonic transducers and that was tested under cyclic loading to failure at EPFL's Structures Laboratory [26.]. The system autonomously localized AE sources and estimated damage mechanisms using Moment Tensor Inversion (MTI), providing both speed and reliability that far exceed traditional manual methods.

SPECIMEN, INSTRUMENTATION, DATA ACQUISITION

The test specimen is a laboratory-scale T-shaped beam fabricated from UHPFRC. It measured 4.2 meter in length, with a 4.0 meters span and a total depth of 0.45 meters. The beam had a web thickness of 75 mm and was cast as a single element at EPFL using a high-performance Swiss UHPFRC mix (Figure 1). The reinforcement included a single 26 mm diameter steel rebar with a minimum yield strength of 435 MPa. More details are provided in [26, 27]. The UHPFRC mix incorporated 3.4% by volume of short, slender steel fibers (13 mm length, 0.16 mm diameter) to enhance toughness and crack resistance. The mix design featured a water/binder ratio of 0.18 and included cement, silica fume, quartz sand (particles <1 mm) from a commercial premix, and superplasticizer. The casting process, which lasted approximately 75 minutes, was carefully sequenced to ensure uniform dispersion of materials and fibers. The age of the UHPFRC was defined from the moment water was added (February 10, 2022, at 12:00), serving as the reference point for all subsequent monitoring. According to Swiss UHPFRC standards [28], the beam was expected to meet grade "UB" mechanical properties, with a tensile strength ≥12 MPa, compressive strength ≥140 MPa, and modulus of elasticity ≥45 GPa. At 28 days, its average density was measured at 2599 kg/m³.

Instrumentation of the beam included 24 embeddable ultrasonic transducers (Model S0807 from ACS), which were randomly positioned within the beam's web. These transducers were oriented perpendicularly to the web surface and held in place using plastic sleeves embedded in the formwork during casting. This transducer network enabled both passive and active ultrasonic stress wave measurements throughout the test.

For data acquisition, a Vallen AMSY-6 system was employed to record both passive and active ultrasonic signals. AE signals were captured using a sampling rate of 10 MHz, with a trigger threshold of 34 dB and a 40 dB preamplifier gain. The analog band-pass filter range was set between 25 and 850 kHz. A maximum of 32,768 samples was recorded per waveform, equivalent to a 3.28 ms recording duration. For active ultrasonic transmission, each transducer emitted four pulses (at 1-second intervals), while the others recorded the waveforms, creating 2,208 individual measurements per pulse sequence. These sequences were repeated every 30 minutes to monitor the evolution of the material's mechanical behavior. To manage data volume and ensure reliability, acquisition was segmented into seven sub-phases, helping avoid data loss and maintain manageable file sizes.

The rigorous specimen preparation with transducer installation, and high-frequency data acquisition approach provided a detailed, high-resolution evaluation of the fracture behavior and evolving mechanical properties of UHPFRC under loading-laying the groundwork for accurate structural health assessment through AE and ultrasonic monitoring techniques.

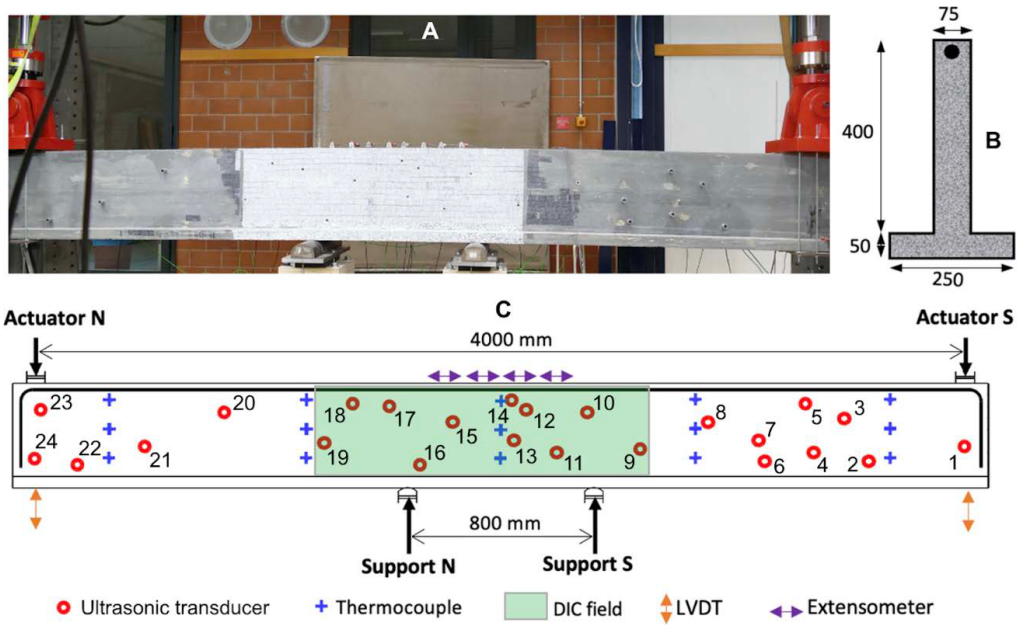

Figure 1. A) Experimental test setup; B) Specimen cross-section; C) instrumentation (Source: [26]).

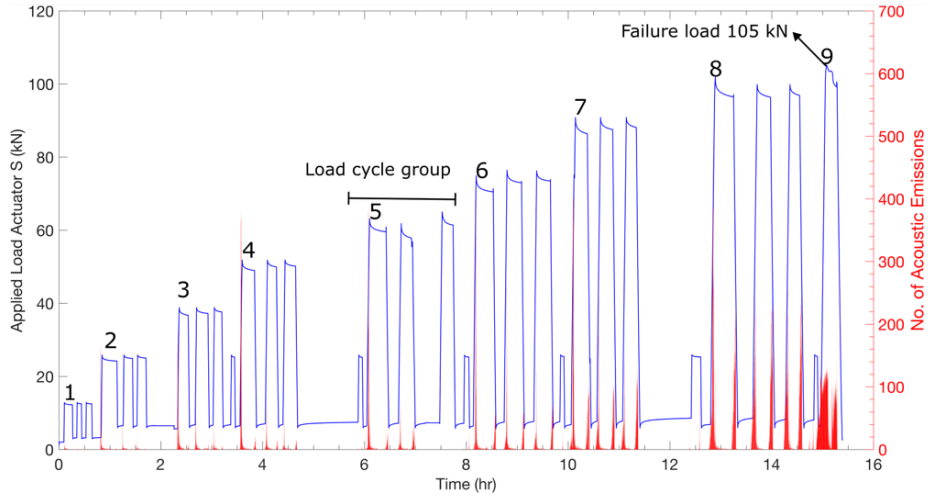

Figure 2. Illustration of loading protocol: Load (Actuator S) vs. time. LCG are numbered with the number being located at the first loading cycle of that group. Detected AEs are shown in red.

LOADING PROTOCOL AND MONITORING PROCEDURE

The specimen was tested under a four-point bending setup following a predefined loading protocol illustrated in Figure 2 (see [26] for details). The loading sequence consisted of repeated load-unload cycles organized into groups called Load Cycle Groups (LCG). Each LCG involved three cycles at a specific peak load, with intermediate single cycles at a representative service load of 26 kN. The peak loads applied during successive LCGs were 13, 26, 39, 52, 65, 78, 91, and 104 kN. The final stage of the test, labeled "F," involved monotonic loading until failure occurred at 105

kN. Displacement-controlled loading was used throughout to maintain stability and minimize dynamic effects.

AE LOCALIZATION USING SIMORGH

The AMSY-6 waveform data of each LCG were processed using SIMORGH. By applying its event association algorithm to over 3.5 million waveforms, we identified more than half a million AE events, of which approximately 300,000 were recorded by at least five transducers. A P-wave velocity of 4700 m/s, estimated from active ultrasonic measurements [26], was used for localization herein.

The localization algorithm employed a guided two-step grid search, beginning with 40 mm resolution and refining to 10 mm. The number of localized AE events per LCG is summarized in Table 1, with representative subsets visualized in Figure 3. The selected AE events included in the analysis were detected by at least five transducers with an azimuthal gap of less than 270°, a travel time RMS error below 10 μs, and a minimum source-to-transducer distance of no more than 350 mm. The complete processing workflow was executed in under 10 hours on nine 3.4 GHz processors using less than 50 GB of RAM.

SIMORGH uses waveform data in both the time and frequency domains for localization. Pre-processing includes several steps such as transducer selection, waveform feature extraction, and phase picking in both domains. For each AE source, additional parameters such as relative magnitude, central frequency, rise time, and duration were computed automatically. Relative magnitudes were determined using the method described in [29], which accounts for signal amplitudes and source-to-transducer distances.

The resulting AE localizations showed spatial distributions consistent with those reported in [26]. Notably, SIMORGH localized more than three times the number of events compared to [26] in each LCG.

TABLE I. RESULTS PER LCG: AE RAW AND PROCESSED DATA

LCG (kN)	Number of traces/events	Localized/Selected AE events	Relative magnitude
13	22,145 / 307	202/139	-3.0/-2.35
26	91,474 / 4,786	1633/322	-3.2/-1.7
39	179,157 / 10,986	5835/1090	-3.1/-0.9
52	215,526 / 15,795	6994/1123	-3.3/-0.8
65	303,088 / 21,185	13346/1255	-3.5/-0.6
78	367,681 / 24,426	11897/1021	-3.3/-0.6
91	666,012 / 44,494	32487/2266	-3.5/-0.3
104	1,210,592 / 79,944	50028/2586	-3.5/-0.1
105	622,976 / 92,536	31421/745	-3.4/-0.8

AE MOMENT TENSOR INVERSION USING SIMORGH

One of the solutions implemented in SIMORGH is the automated inversion of AE P-wave first-motion polarities and their initial amplitudes to obtain both full and deviatoric moment tensor solutions, following methodologies inspired by [30, 31]. This

tensor represents the components of stress at the source, which gives the rupture-damage mechanism, useful for structural evaluation and risk prevention.

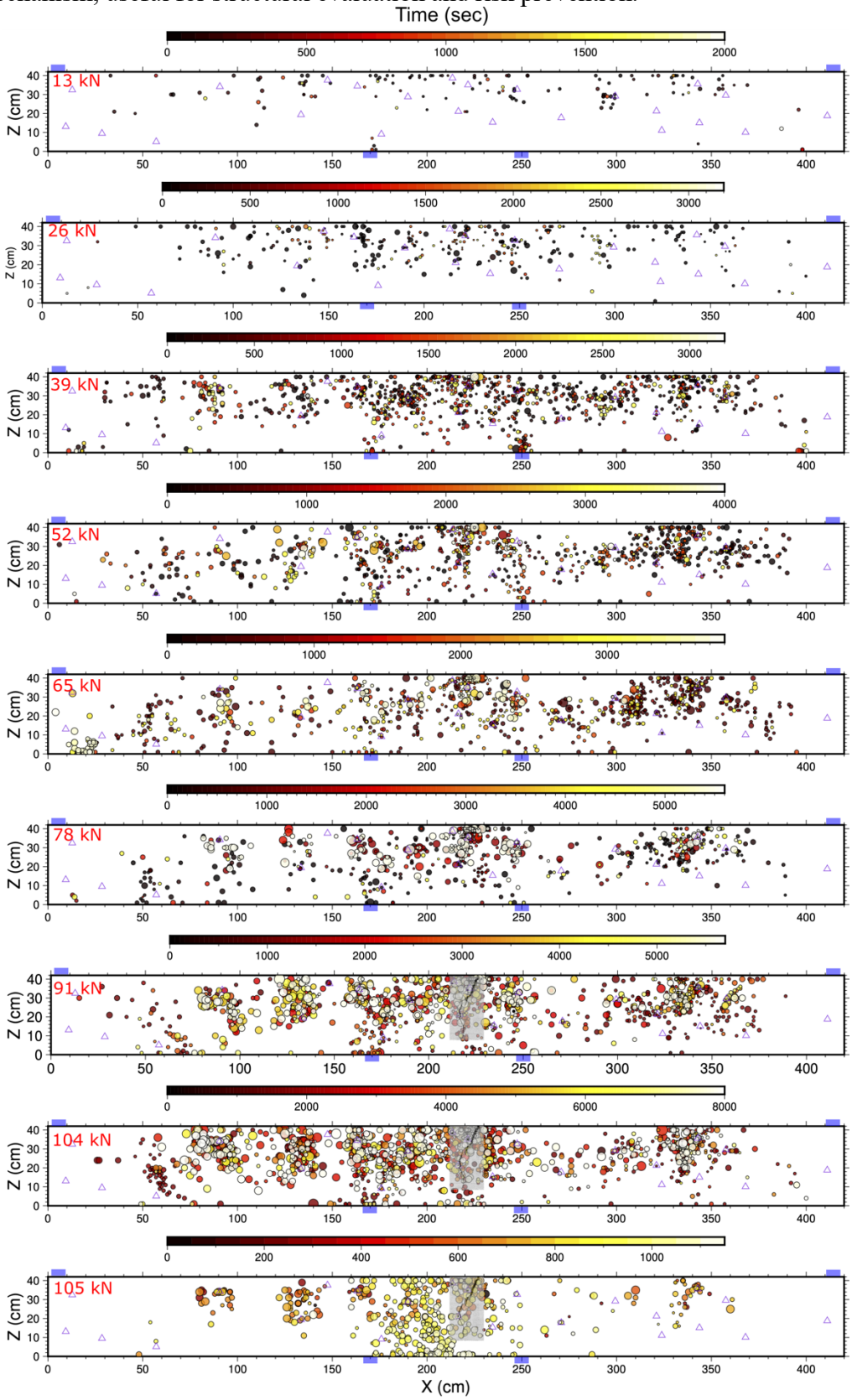

Figure 3. Selected AE source locations (colored circles) for LCG 1 to 9. Crack geometries measured at the end of LCG 7-9 are plotted on top of AE sources, for reference. Triangles represent transducer locations. Purple rectangles show actuators on the top and supports on the bottom of the beam.

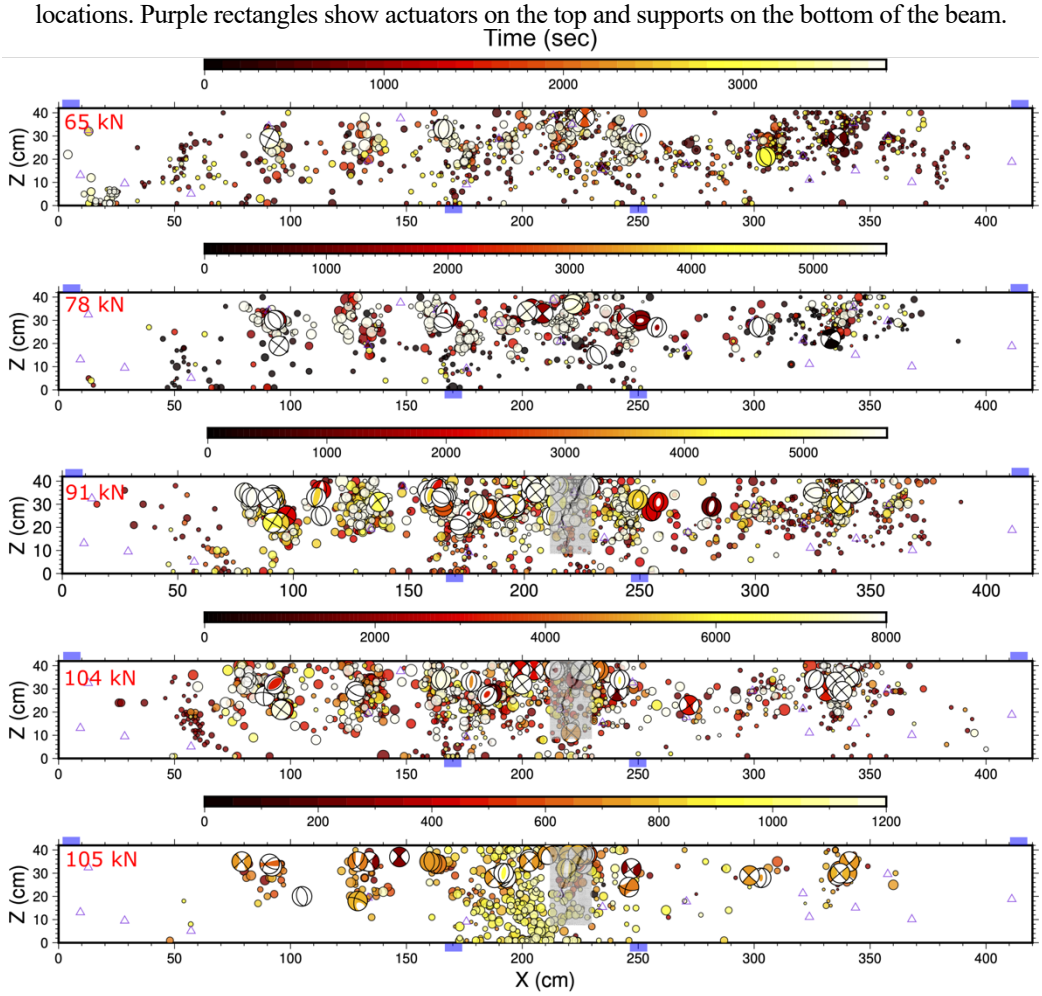

Figure 4. Selected focal mechanisms for the LCG 5 to 9.

This method requires proper azimuthal coverage of transducers to reliably resolve the seismic radiation pattern. We selected AE events with a minimum of eight polarity readings and an azimuthal coverage of at least 180°. To enhance accuracy, the algorithm was configured to search for the hypocenter in 3D, including the 75 mm beam web as the third axis. The MTI was constrained to a deviatoric solution (ISO component = 0) to reduce the number of degrees of freedom in the inversion. Solution stability was assessed through multiple tests per AE, including Jackknife resampling and scalar seismic moment (M_0) error estimation. For final selection, nodal planes were permitted to rotate by no more than 20°, and a maximum of one reverse polarity was tolerated. The selected moment tensors for each load stage exhibit consistency with the AE distribution (see Figure 4). Most of the computed MTs correspond to the later phases of each load stage, when the largest AEs occurred.

DISCUSSION

Accurate localization of AE sources requires careful signal pre-processing, reliable implementation of a velocity model, and selection of appropriate localization algorithms. Manual seismic-acoustic localization has traditionally been considered the most precise method for fracture monitoring. However, this approach typically requires 1–3 minutes per event, depending on the number of transducers (typically 8–20) and the signal quality needed to pick P- and S-wave arrivals. Weaker AEs would require other approaches such as template matching for proper localization. While AI-based methods offer faster processing post-training, they generally do not reach the same level of precision.

SIMORGH-SHM localizes AE sources in a fraction of a second, leveraging all available processors in the system. Its hybrid algorithm manages each processing stage including method selection, signal conditioning, feature extraction in both time and frequency domains, and multiple quality control steps, to deliver real-time, high-precision fracture monitoring. The algorithm comprises over 50 tunable hyperparameters, optimized according to project-specific conditions. In addition to damage source localization, SIMORGH also estimates source mechanisms.

The AE results processed in this study are consistent with those obtained using the traditional Geiger method, as reported in [26, 27], which is also implemented as one of the available methods in SIMORGH's core algorithm. As the applied load increases, both the number and magnitude of AE events grow. During the early loading stages (up to LCG 3), AE activity is sparsely distributed, eventually concentrating around the emerging fracture zones as damage localizes. The obtained crack geometry by digital image correlation (DIC) [26] also matches the distribution of the main cluster of AE sources (Figure 3). The main distribution of AE sources can be observed within the two support points and in the middle of each support point and the respective actuator. AE sources on the northern side of the beam are aligned showing possible crack dipping to the south and vice versa.

The automatically calculated moment tensors of AE sources show main opening and shearing mechanisms, and despite the challenging transducer coverage for this method, their corresponding nodal planes are consistent with the elongated AEs. The multilayer algorithm of SIMORGH enables detailed analysis of fracture mechanisms in near real time.

CONCLUSION AND FUTURE WORK

SIMORGH significantly reduces the cost and time associated with AE source localization and moment tensor inversion, while maintaining high precision. It enables real-time monitoring capabilities with large number of transducers that are currently lacking but critically needed in several SHM and NDE applications where tracking fracture growth is essential. The near-real-time localization and MTI solution supports timely decision-making, setting a new standard for structural safety.

The next step in this research involves integrating SIMORGH's near-real-time ultrasonic tomography module with the available active ultrasonic stress wave measurements and incorporating the resulting dynamic velocity models into real-time AE hypocenter localization.

By enabling reliable and cost-effective deployment of AE surveillance arrays, SIMORGH promotes broader adoption of continuous monitoring systems, ultimately

enhancing public safety. In summary, this software represents a major advancement with the potential to improve structural security, environmental sustainability, and community resilience.

ACKNOWLEDGEMENT

This work is supported by the Swiss National Science Foundation (SNSF), Innosuisse grant number: 119.735 IP-EE. The experiment was conducted in the EPFL Structural Engineering Platform (GIS). Technical support for formwork and specimen fabrication as well as instrumentation was provided by Gilles Guignet (technical coordinator), François Perrin, Léa Frédérique Dubugnon, and Luca Mari.

REFERENCES

1. Habel, K., Viviani, M., Denari´e, E., & Brühwiler, E. (2006). Development of the mechanical properties of an ultra-high performance fiber reinforced concrete (UHPFRC). Cement and Concrete Research, 36(7), 1362–1370. https://doi.org/10.1016/j.cemconres.2006.03.009.
2. F.A. Farhat, D. Nicolaides, A. Kanellopoulos, et al., High performance fibre-reinforced cementitious composite (CARDIFRC) – _performance and application to retrofitting, Eng. Fract. Mech. 74 (2007) 151–167.
3. M. Qiu, X. Shao, K. Wille, et al., Experimental investigation on flexural behavior of reinforced ultra high performance concrete low-profile T-beams, Int J. Concr. Struct. Mater. 14 (2020) 5.
4. B. Sawicki, E. Brühwiler, E. Denari´e, Inverse analysis of R-UHPFRC members to determine the flexural response underservice loading and at ultimate resistance, J. Struct. Eng. 148 (2020) 040221260.
5. Bertola, N., Schiltz, P., Denarié, E., & Brühwiler, E. (2021). A Review of the Use of UHPFRC in Bridge Rehabilitation and New Construction in Switzerland. *Frontiers in Built Environment*, 7, 769686.
6. Graybeal, B. A. (2020). *International Perspective on UHPC in Bridge Engineering*. *Journal of Bridge Engineering*, 25(11), 04020094.
7. K. Habel, M. Viviani, E. Denari´e, et al., Development of the mechanical properties of an ultra-high performance fiber reinforced concrete (UHPFRC), Cem. Concr. Res. 36 (2006) 1362–1370.
8. D.-Y. Yoo, S.-T. Kang, J.-H. Lee, et al., Effect of shrinkage reducing admixture on tensile and flexural behaviors of UHPFRC considering fiber distribution characteristics, Cem. Concr. Res 54 (2013) 180–190.
9. Kazemi Kamyab M. Autogenous Shrinkage and Hydration Kinetics of SH-UHPFRC under Moderate to Low Temperature Curing Conditions. EPFL, 2013. Epub ahead of print 2013. DOI: 10.5075/epfl-thesis-5681.
10. K. Habel, P. Gauvreau, Response of ultra-high performance fiber reinforced concrete (UHPFRC) to impact and static loading, Cem. Concr. Compos. 30 (2008) 938–946.
11. J.-Y. Wang, J.-Y. Guo, Damage investigation of ultra high performance concrete under direct tensile test using acoustic emission techniques, Cem. Concr. Compos. 88 (2018) 17–28.
12. P.R. Prem, M. Verma, A.R. Murthy, et al., Smart monitoring of strengthened beams made of ultrahigh performance concrete using integrated and nonintegrated acoustic emission approach, Struct. Control Health Monit. 28 (2021) e2704.
13. S. Li, L. Zhang, P. Guo, et al., Characteristic analysis of acoustic emission monitoring parameters for crack propagation in UHPC-NC composite beam under bending test, Constr. Build. Mater. 278 (2021) 122401.
14. K. Naukhez, J.M. Kishen, R. VS, Observations on the characteristics of acoustic emissions generated during unconfined uniaxial compression of ultra high performance concrete, J. Struct. Eng. Madras 48 (2021) 393–403.
15. C. Chen, X. Chen, Y. Ning, Identification of fracture damage characteristics in ultra-high performance cement-based composite using digital image correlation and acoustic emission techniques, Compos. Struct. 291 (2022) 115612.

16. X. Xu, Z. Jin, Y. Yu, et al., Damage source and its evolution of ultra-high performance concrete monitoring by digital image correlation and acoustic emission technologies, J. Build. Eng. 65 (2023) 105734.
17. X. Wang, D. Liu, Y. Zhang, et al., Fracture Characterization of ultra-high performance concrete Notched beams under the Influence of different material factors based on acoustic emission technique, Materials 14 (2021) 4608.
18. J.-Y. Wang, Z.-Z. Chen, K. Wu, Properties of calcium sulfoaluminate cement made ultra-high performance concrete: Tensile performance, acoustic emission monitoring of damage evolution and microstructure, Constr. Build. Mater. 208 (2019) 767–779.
19. X. Wang, E. Niederleithinger, I. Hindersmann, The installation of embedded ultrasonic transducers inside a bridge to monitor temperature and load influence using coda wave interferometry technique, Struct. Health Monit. 21 (2022) 913–927.
20. A. Bassil, X. Wang, X. Chapeleau, et al., Distributed fiber optics sensing and coda wave interferometry techniques for damage monitoring in concrete structures, Sensors 19 (2019) 356.
21. N. Burud, J.C. Kishen, Damage detection using wavelet entropy of acoustic emission waveforms in concrete under flexure, Struct. Health Monit. 20 (2021) 2461–2475.
22. Momeni, S., D. Liu, and B. Lecampion. 2021. "Combining active and passive acoustic methods to image hydraulic fracture growth in laboratory experiments". *Eurock21*, Turin, Italy, DOI:10.1088/1755-1315/833/1/012088.
23. Momeni, S., G. Lu, and B. Lecampion, 2021. "Automatic passive acoustic emission-microseismic monitoring using a parallel algorithm; A case study of a hydraulic-fracturing experiment" *SGM 19*, Geneva, Switzerland.
24. Momeni, S., T. Schumacher, L. Linzer, B. Lecampion, 2023. "Automatic and high-precision acoustic emission-based structural health monitoring of concrete structures" *IWSHM2023*, Stanford, CA, USA.
25. Momeni, S., Schumacher, T., Linzer, L., & Lecampion, B. (2024). Advanced Acoustic Emission-based SHM for Concrete Structures: Real-Time, High-Precision Imaging of Crack Geometry and Damage Source-type Using Moment Tensor Inversion. In *Proceedings of the 11th European Workshop on Structural Health Monitoring (EWSHM 2024)*.
26. Bertola, N. J., Schumacher, T., Niederleithinger, E., & Brühwiler, E. (2024). Early detection of structural damage in UHPFRC structures through the combination of acoustic emission and ultrasonic stress wave monitoring. In 11th European Workshop on Structural Health Monitoring (EWSHM 2024).
27. Bertola, N., Schumacher, T., Niederleithinger, E., & Brühwiler, E. (2025). Combining passive and active ultrasonic stress wave monitoring for the characterization of the early-age properties of a UHPFRC beam. *Construction and Building Materials, 466*, 140319. https://doi.org/10.1016/j.conbuildmat.2025.140319
28. SIA (2016). *SIA 2052:2016 — Béton fibré ultra-performant (BFUP): Matériaux, dimensionnement et exécution*. Zurich, Switzerland: Société suisse des ingénieurs et des architectes (SIA).
29. Zang, A., Wagner, C., Stanchits, S., Dresen, G., Andresen, R., & Haidekker, M. (1998). Source analysis of acoustic emissions in Aue granite cores under symmetric and asymmetric compressive loads. Geophysical Journal International, 135, 1113-1130. (https://doi.org/10.1046/j.1365-246X.1998.00706.x).
30. Fitch, T. J., D. W. McCowan, and M. W. Shields (1980). Estimation of seismic moment tensor from teleseismic body wave data with application to intraplate and mantle earthquakes, J. Geophys. Res. 85, 3817–3828.
31. Andersen, L. M. (2001). A Relative Moment Tensor Inversion Technique Applied to Seismicity Induced by Mining, Univ. of the Witwatersrand, Johannesburg.